Uncooled $InAs_{0.09}Sb_{0.91}$ photoconductors with cutoff wavelength extended to 11.5 μm*

GAO Yu-zhu (高玉竹)[1]**, **GONG Xiu-ying** (龚秀英)[1], **ZHOU Ran** (周冉)[1], **LI Ji-jun** (李继军)[2], **FENG Yan-bin** (冯彦斌)[2], **Takamitsu Makino**[3], **and Hirofumi Kan**[3]

1. College of Electronics and Information Engineering, Tongji University, Shanghai 201804, China

2. Huaxing Infrared Device Company, Xi'an 712099, China

3. Hamamatsu Photonics K. K., 5000 Hirakuchi, Hamakita 434-8601, Japan

(Received 1 July 2015)

Uncooled InAsSb photoconductors were fabricated. The photoconductors were based on $InAs_{0.05}Sb_{0.95}$ and $InAs_{0.09}Sb_{0.91}$ thick epilayers grown on InAs substrates by melt epitaxy (ME). Ge immersion lenses were set on the photoconductors. The cutoff wavelength of $InAs_{0.09}Sb_{0.91}$ detectors is obviously extended to 11.5 μm, and that of $InAs_{0.05}Sb_{0.95}$ detectors is 8.3 μm. At room temperature, the peak detectivity of $D_{\lambda p}$* at wavelength of 6.8 μm and modulation frequency of 1 200 Hz is 1.08×10^9 cm·Hz$^{1/2}$·W^{-1} for $InAs_{0.09}Sb_{0.91}$ photoconductors, the detectivity D* at wavelength of 9 μm is 7.56×10^8 cm·Hz$^{1/2}$·W^{-1}, and that at 11 μm is 3.92×10^8 cm·Hz$^{1/2}$·W^{-1}. The detectivity of $InAs_{0.09}Sb_{0.91}$ detectors at the wavelengths longer than 9 μm is about one order of magnitude higher than that of $InAs_{0.05}Sb_{0.95}$ detectors, which rises from the increase of arsenic (As) composition in $InAs_{0.09}Sb_{0.91}$ materials.

Document code: A **Article ID:** 1673-1905(2015)05-0352-4

DOI 10.1007/s11801-015-5122-y

The wavelength range of 8–12 μm is a very important infrared (IR) atmospheric window. HgCdTe detector is the dominant system in the long wavelength IR waveband. However, it suffers from chemical instability and nonuniformity due to the high Hg vapor pressure during its growth. InAsSb alloy with long wavelength has high electron and hole mobilities, good mechanical strength and chemical stability, and good working characteristics at room temperature. Therefore, it becomes a very attractive material alternative compared with HgCdTe alloy[1-3]. However, the lattice mismatch between the InAsSb epilayers with long wavelength and the binary compound substrates is rather large, which is larger than 6% for InAs, and is 7.2%–14.6% for GaAs. Therefore, it is difficult to grow long wavelength InAsSb single crystals with high quality. In order to obtain long wavelength InAsSb type-Ⅱ superlattice detectors with high performance, the liquid nitrogen cooler is needed and the operations are at temperature below 150 K[1-3]. At 77 K, the device in Ref.[1] is reverse biased at 150 mV, and the peak detectivity reaches 1.4×10^{10} cm·Hz$^{1/2}$·W^{-1} at the wavelength of 12.8 μm.

In our previous papers, the InAsSb thick epilayers with cutoff wavelengths longer than 8 μm were grown on InAs substrates by melt epitaxy (ME)[4-11]. The thickness of the epilayers reaches 100 μm. This thickness effectively suppresses the affection of the lattice mismatch, and results in a low dislocation density at the order of 10^4 cm^{-2} and good crystal quality of the epilayers. However, the cutoff wavelength of uncooled $InAs_{0.05}Sb_{0.95}$ detectors grown by ME is 8.3 μm[10]. In this paper, the cutoff wavelength of $InAs_{0.09}Sb_{0.91}$ photoconductors is extended to 11.5 μm, which is obviously longer than that of $InAs_{0.05}Sb_{0.95}$ detectors. It is caused by arsenic (As) composition increase in the epilayers. At room temperature, the peak detectivity $D_{\lambda p}$* at the wavelength of 6.8 μm reaches 1.08×10^9 cm·Hz$^{1/2}$·W^{-1}, the detectivity D* at 10 μm is 5.40×10^8 cm·Hz$^{1/2}$·W^{-1}, and that at 11 μm is 3.92×10^8 cm·Hz$^{1/2}$·W^{-1} for $InAs_{0.09}Sb_{0.91}$ immersed detectors.

InAsSb epilayers were grown on (100)-oriented n-InAs substrates in a horizontal liquid phase epitaxy (LPE) growth system in high purity hydrogen ambient. The source materials were 7N (99.999 99%) antimony (Sb), indium (In) and non-doped InAs single crystals. The size of InAs substrates was 9 mm×11 mm. The grown of epilayers on the substrates with larger size should be further studied. The detailed growth process of ME has been published in our previous paper[5]. The key point is as follows: at the growth temperature of about 500 °C, the melt was pushed to contact with the substrate, and the excess growth melt was immediately removed away from the substrate by pushing the melt holder. It is important that some melt was remained on the surface of

* This work has been supported by the Fundamental Research Funds for the Central Universities in China.

** E-mail: gaoyuzhu@tongji.edu.cn

the substrate at the growth temperature. Then the substrate was pushed under the flat part (the block) of the melt holder and cooled with a cooling rate of 0.5 °C/min to obtain an epilayer. X-ray diffraction (XRD) patterns of the InAsSb samples were measured by an X-ray diffractometer (BRUKER D8 ADVANCE, Cu barn) at a voltage of 40 kV and a current of 40 mA. Transmittance measurements for the samples were performed using a Fourier transform infrared (FTIR) spectrophotometer (SHIMADZU IRPRESTIGE-21).

The uncooled photoconductors were fabricated based on $InAs_{0.05}Sb_{0.95}$ and $InAs_{0.09}Sb_{0.91}$ thick epilayers grown by ME. InAs substrates were entirely removed away during the process. Thus the influence of the lattice mismatch between epilayers and substrates was eliminated. Ge immersion lenses were set on the photoconductors. The area of the sensitive elements is 0.05 cm×0.05 cm. In was employed as the electrode. At room temperature, the spectral photoresponse of InAsSb photoconductors was measured by an FTIR spectrometer, and the absolute responsivity was calibrated by a standard blackbody source at the temperature of 500 K and the modulation frequency of 1 200 Hz. The bias current applied on the detectors was 10 mA.

Fig.1 shows the XRD pattern for an InAs/$InAs_{0.09}Sb_{0.91}$ sample. As shown in Fig.1, Cukα1 and Cukα2 diffraction peaks of InAsSb epilayers are clearly observed, and no other crystal structure appears. The growth direction of the epilayers agrees with the surface direction of InAs substrates, i.e., the (100) orientation. It demonstrates that InAsSb epilayers are indeed single crystals. The sharpness and the full-width at half-maximum (*FWHM*) of the InAsSb (400) Cukα1 diffraction peak (263″) both indicate the high quality of the epilayers.

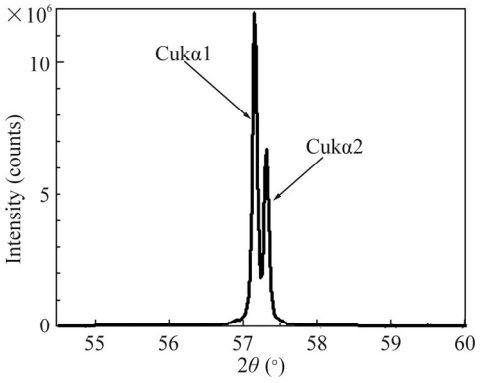

Fig.1 XRD pattern of an InAs/$InAs_{0.09}Sb_{0.91}$ sample

According to the Bragg diffraction equation, the lattice constant for $InAs_xSb_{1-x}$ samples shown in Fig.1 is estimated to be 0.644 10 nm. Based on Vegard law[12], the mole fraction of As in the epilayers can be estimated by

$$x = (a_{\mathrm{InAsSb}} - a_{\mathrm{InSb}}) / (a_{\mathrm{InAs}} - a_{\mathrm{InSb}}), \quad (1)$$

where x is the mole fraction of As in the epilayers, and a is the lattice constant. The mole fraction of As is estimated to be 0.09 for the sample in Fig.1. The atomic fraction of As in the epilayer measured by EPMA is 9.1%, which is in agreement with that obtained by XRD measurement. The lattice constant of $InAs_{0.09}Sb_{0.91}$ (0.644 10 nm) is smaller than that of InSb (0.647 89 nm). It indicates the lattice compression of InAsSb crystals grown by ME due to As atoms substitution in the lattice. The lattice mismatch between $InAs_{0.09}Sb_{0.91}$ epilayers and InAs substrates is 6.31%.

Fig.2 shows the transmittance spectra of $InAs_{0.05}Sb_{0.95}$ and $InAs_{0.09}Sb_{0.91}$ samples. In Fig.2, the intrinsic absorption edges appear at the wavelength of 8.0 μm and 9.5 μm for $InAs_{0.05}Sb_{0.95}$ and $InAs_{0.09}Sb_{0.91}$ samples, respectively. It is clear red shift for $InAs_{0.09}Sb_{0.91}$ sample. As shown in Fig.4, the obvious photoresponse is observed beyond 8.0 μm and 9.5 μm for the photoconductors made from $InAs_{0.05}Sb_{0.95}$ and $InAs_{0.09}Sb_{0.91}$ epilayers, respectively.

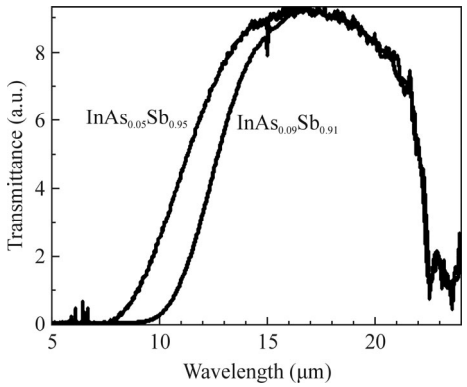

Fig.2 Transmittance spectra of $InAs_{0.05}Sb_{0.95}$ and $InAs_{0.09}Sb_{0.91}$ samples at room temperature

The variation of $(\alpha h\nu)^2$ with $h\nu$ is shown in Fig.3, where α is absorption coefficient, and $h\nu$ is incident photon energy. In Fig.3, the optical band gaps of $InAs_{0.05}Sb_{0.95}$ sample and $InAs_{0.09}Sb_{0.91}$ sample are estimated to be 0.14 eV and 0.11 eV by linear fitting, respectively.

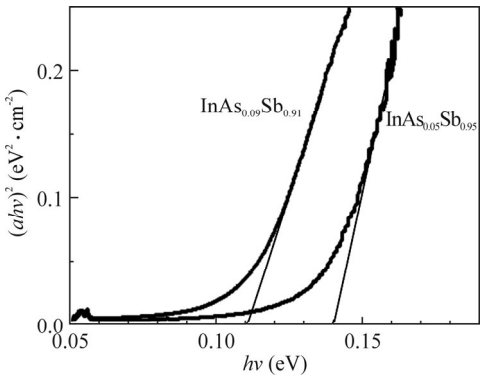

Fig.3 Variation of $(\alpha h\nu)^2$ with $h\nu$ for $InAs_{0.05}Sb_{0.95}$ and $InAs_{0.09}Sb_{0.91}$ samples

Fig.4 shows the spectral photoresponse curves of an

uncooled $InAs_{0.05}Sb_{0.95}$ photoconductor with SiO antireflective coating labeled by sample a and an uncooled $InAs_{0.09}Sb_{0.91}$ photoconductor without any antireflective coating labeled by sample b. Ge immersion lenses were set on the photoconductors. The cutoff wavelength of detector is usually defined as the wavelength at 20% of the peak response. In Fig.4, the cutoff wavelengths of samples a and b are 8.3 μm and 11.5 μm, respectively. The corresponding band gaps of $InAs_{0.05}Sb_{0.95}$ and $InAs_{0.09}Sb_{0.91}$ detectors are 0.149 4 eV and 0.107 8 eV, which are close to 0.14 eV and 0.11 eV estimated in Fig.3. The band gaps of the InAsSb samples are narrower than that of InSb (0.17 eV), which mainly results from the lattice contraction due to the incorporation of As in the lattice. The lattice constant of $InAs_{0.09}Sb_{0.91}$ epilayer (0.644 10 nm) is smaller than that of $InAs_{0.05}Sb_{0.95}$ epilayer (0.645 72 nm), which leads to the narrower band gap of $InAs_{0.09}Sb_{0.91}$ detector (sample b). Additionally, the non-regular arrangement of atoms in the lattice may also affect the energy band bowing for III-V mixed crystals.

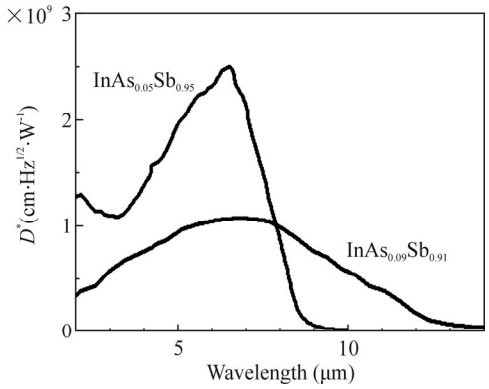

Fig.4 Spectral photoresponse curves of an uncooled $InAs_{0.05}Sb_{0.95}$ photoconductor with SiO antireflective coating labeled by sample a and an uncooled $InAs_{0.09}Sb_{0.91}$ photoconductor without any antireflective coating labeled by sample b

At room temperature, the peak responsivity $R_{\lambda p}$ is 164.3 V/W at the wavelength of 6.5 μm for sample a, and that is 70.9 V/W at the wavelength of 6.8 μm for sample b. The peak detectivity $D_{\lambda p}$* (6.5 μm, 1 200 Hz) is 2.50×10^9 cm·Hz$^{1/2}$·W^{-1} for sample a, and $D_{\lambda p}$* (6.8 μm, 1 200 Hz) is 1.08×10^9 cm·Hz$^{1/2}$·W^{-1} for sample b. The peak detectivity $D_{\lambda p}$* of sample a is higher than that of sample b, since there is SiO antireflective coating on detector a, while there is not any antireflective coating on detector b. The antireflective coating improves the detectivity of detector a.

However, the detectivities D* are 6.54×10^7 cm·Hz$^{1/2}$·W^{-1} and 2.25×10^7 cm·Hz$^{1/2}$·W^{-1} at the wavelength of 9 μm and 10 μm for sample a, and those are 7.56×10^8 cm·Hz$^{1/2}$·W^{-1} and 5.40×10^8 cm·Hz$^{1/2}$·W^{-1} at 9 μm and 10 μm for sample b, respectively. The detectivities at 9 μm and 10 μm of $InAs_{0.09}Sb_{0.91}$ detector are about one order of magnitude higher than those of $InAs_{0.05}Sb_{0.95}$ detector. The detectivity at the wavelength of 11 μm is 3.92×10^8 cm·Hz$^{1/2}$·W^{-1} for sample b. The improvement of the detectivity with the wavelengths longer than 9 μm for sample b results from the more As composition in $InAs_{0.09}Sb_{0.91}$ epilayer.

The good sensitivity of uncooled InAsSb detectors is possibly caused by the following reasons. Firstly, the immersion Ge lenses were set on our photoconductors. The incident IR radiation was focused by the lenses, and thus the radiation energy density on the photosensitive surfaces was raised. The immersion lens can raise the signal-to-noise ratio and the detectivity by approximately one order of magnitude. Secondly, InAsSb epilayers with the thickness of 100 μm grown by ME have the properties of narrow-gap bulk single crystals. The intrinsic semiconductors are more suitable for uncooled photodetectors with long wavelength. The high density of states in the valence and conduction bands of them result in the strong absorption of IR radiation[13]. Additionally, the response time of uncooled InAsSb photodetectors is at the order of magnitude of 10^{-1} μs, which is at least three orders of magnitude faster than that of heat IR detectors.

In summary, the immersed photoconductors were made from $InAs_{0.05}Sb_{0.95}$ and $InAs_{0.09}Sb_{0.91}$ thick epilayers on InAs substrates grown by ME. Spectral photoresponse curves of the detectors show that the cutoff wavelength of $InAs_{0.09}Sb_{0.91}$ detector is red-shifted to 11.5 μm, which is remarkably longer than that of 8.3 μm for $InAs_{0.05}Sb_{0.95}$ detector. The strong narrowing of band gap results from the increase of As composition in the epilayers. At room temperature, the peak detectivity at the wavelength of 6.8 μm is 1.08×10^9 cm·Hz$^{1/2}$·W^{-1}, and the detectivities are 5.40×10^8 cm·Hz$^{1/2}$·W^{-1} and 3.92×10^8 cm·Hz$^{1/2}$·W^{-1} at 10 μm and 11 μm for $InAs_{0.09}Sb_{0.91}$ photoconductor, respectively. The measurement results indicate the possible applications for long wavelength IR detections.

References

[1] A. M. Hoang, G. Chen, R. Chevallier, A. Haddadi and M. Razeghi, Applied Physics Letters **104**, 251105 (2014).

[2] A. Haddadi, G. Chen, R. Chevallier, A. M. Hoang and M. Razeghi, Applied Physics Letters **105**, 121104 (2014).

[3] H. S. Kim, O. O. Cellek, Zhi-Yuan Lin, Zhao-Yu He, Xin-Hao Zhao, Shi Liu, H. Li and Y.-H. Zhang, Applied Physics Letters **101**, 161114 (2012).

[4] Y. Z. Gao, X. Y. Gong, H. Kan, M. Aoyama and T. Yamaguchi, Japanese of Journal of Applied Physics **38**, 1939 (1999).

[5] Y. Z. Gao, H. Kan, F. S. Gao, X. Y. Gong and T. Yamaguchi, Journal of Crystal Growth **234**, 85 (2002).

[6] Y. Gao, H. Kan and T. Yamaguchi, Crystal Research and Technology **35**, 943 (2000).

[7] Y. Z. Gao, H. Kan, M. Aoyama and T. Yamaguchi,

Japanese of Journal of Applied Physics **39**, 2520 (2000).

[8] Yu-zhu Gao, Xiu-ying Gong, Guang-hui Wu, Yan-bin Feng, Takamitsu Makino, Hirofumi Kan, Tadanobu Koyama and Yasuhiro Hayakawa, International Journal of Minerals, Metallurgy, and Materials **20**, 393 (2013).

[9] Yuzhu Gao, Xiuying Gong, Takamitsu Makino, Hirofumi Kan, Guanghui Wu, Yanbin Feng, Tadanobu Koyama and Yasuhiro Hayakawa, Advanced Materials Research **668**, 664 (2013).

[10] GAO Yu-zhu, GONG Xiu-ying, LI Ji-jun, WU Guang-hui, FENG Yan-bin, Takamitsu Makino and Hirofumi Kan, Journal of Optoelectronics·Laser **26**, 825 (2015). (in Chinese)

[11] GAO Yu-zhu, GONG Xiu-ying, WU Guang-hui, FENG Yan-bin and FANG Wei-zheng, Journal of Optoelectronics·Laser **21**, 1751 (2010). (in Chinese)

[12] A. R. Denton and N. W. Ashcroft, Physical Review A **43**, 3161 (1991).

[13] J. Piotrowski and A. Rogalski, Infrared Physics & Technology **46**, 115 (2004).